In situ observation of reversible domain switching in aged Mn-doped BaTiO$_3$ single crystals

L. X. Zhang[1,2,3] and X. Ren[1,2,*]

[1]*Multi-Disciplinary Materials Research Center, Xi'an Jiaotong University, Xi'an 710049, People's Republic of China*
[2]*Materials Physics Group, National Institute for Materials Science, Tsukuba, 305-0047 Ibaraki, Japan*
[3]*State Key Laboratory for Mechanical Behavior of Materials, Xi'an Jiaotong University, Xi'an 710049, People's Republic of China*

Very recently, a giant recoverable electrostrain effect has been found in aged Fe-doped BaTiO$_3$ single crystals; this effect is based on a defect-mediated *reversible* domain-switching mechanism. However, the reversible domain-switching process itself is yet to be directly verified. In the present study, we performed *in situ* domain observation during electric field cycling for an aged Mn-doped BaTiO$_3$ single crystal and simultaneously measured its polarization (P)–field (E) hysteresis loop. In addition, the electrostrain behavior of the sample was also characterized. Such experimentation made it possible to correlate the mesoscopic domain-switching behavior with the macroscopic properties. It was found that the aged sample shows a remarkable reversible domain switching during electric field cycling; it corresponds very well to a "double" hysteresis loop and a giant recoverable electrostrain effect (with a maximum strain of 0.4%). This provides direct mesoscopic evidence for our reversible domain-switching mechanism. By contrast, an unaged sample shows irreversible domain-switching behavior during electric field cycling; it corresponds to a normal hysteresis loop and a butterfly-type irrecoverable electrostrain behavior. This indicates that the reversible domain switching in the aged sample is related to point-defect migration during aging. We further found that the large recoverable strain is available over a wide frequency range. This is important for the application of this electrostrain effect.

I. INTRODUCTION

Ferroelectric crystals exhibit a spontaneous polarization ($\mathbf{P}_S$) due to a symmetry-lowering transition at a critical temperature (Curie temperature T_C).[1] $\mathbf{P}_S$ can align along one of the several symmetry-allowed orientations, and a region with the same $\mathbf{P}_S$ is called a domain. One domain state can be switched to another (180° reversal or non-180° rotation) by an external electric field.[2] Such domain switching, especially the non-180° one, can generate a huge nonlinear electrostrain due to the exchange of different crystallographic axes.[3] This nonlinear strain may be in theory tens of times larger than the linear (converse) piezoelectric strain. Unfortunately, the domain-switching process is inherently irreversible due to the energetic equivalence of different domain states. Therefore, the large electrostrain caused by domain switching is only a one-time effect, and thus has no practical applications. However, if domain switching can be somehow made reversible, a large *recoverable* electrostrain would be expected.

Very recently, we proposed a principle to realize *reversible domain switching* in a crystal containing point defects.[4] The main idea of this principle is that point defects have a so-far-unrecognized "statistical symmetry" which follows the crystal symmetry when in equilibrium (in short, it is called the defect symmetry principle).[4–8] The symmetry-conforming property of point defects provides an intrinsic restoring force for reversible domain switching.[4,8] Based on this defect-mediated reversible domain-switching mechanism, a giant recoverable electrostrain of 0.75% has been achieved in aged Fe-doped BaTiO$_3$ single crystals[4] and a large electrostrain of 0.12% was achieved in aged Mn-doped (Ba, Sr)TiO$_3$ ceramics.[8] However, direct evidence for the existence of the underlying reversible domain-switching process is yet to be obtained.

In the present study, we performed an *in situ* observation on the domain-switching process during electric field cycling for aged Mn-doped BaTiO$_3$ single crystals, aiming to verify the reversibility of the actual domain-switching process. We devised a special experimental setup that can simultaneously record the mesoscopic domain pattern evolution and measure the macroscopic *P-E* hystersis loop. Such a technique, being different from others,[9,10] provides a direct link between the macroscopic property and the underlying mesoscopic domain-switching behavior. In addition, electrostrain was also measured subsequently together with the *P-E* hysteresis loop. Consequently the correlation among domain-switching behavior, polarization rotation, and electrostrain can be unambiguously established.

In order to prove that the reversible domain-switching behavior in the aged sample is related to defect symmetry, we also performed the same *in situ* experiment for unaged samples. A comparison of the different domain-switching behavior between aged and unaged samples will reveal the underlying microscopic mechanism related to point-defect migration (required by the defect symmetry principle) during aging.

This paper is arranged in the following way. First the symmetry principle of point defects is introduced, which is the basis for understanding the origin of the aging-induced reversible domain switching and corresponding macroscopic properties. Then the experimental setup is described, which is followed by experimental results. Finally we discuss some key points concerning the defect symmetry, domain switching, and macroscopic properties, as well as compare our mechanism with previous ones.

II. DEFECT SYMMETRY PRINCIPLE

Here we give a brief introduction to the defect symmetry principle. This principle was first proposed in the ferroelastic martensites, and explained the similar reversible domain-switching phenomenon in aged ferroelastic martensite alloys.[5–7] Very recently it has been extended to ferroelectrics.[4,8] In the following, we will take the ferroelectric $BaTiO_3$ crystal (which has a simple perovskite structure) as an example to explain this principle.

The defect symmetry principle describes a so-far-unrecognized relationship between crystal symmetry and the "symmetry" of statistical short-range-order distribution of point defects (point defects include dopants, impurities, and vacancies). Here we consider a Mn^{3+}-doped $BaTiO_3$ crystal. Mn^{3+} ions occupy Ti^{4+} sites due to the similarity in ionic radius. To maintain charge neutrality, O^{2-} vacancies are necessarily produced at O^{2-} sites.[11] Consequently we have Mn^{3+} dopants and O^{2-} vacancies as point defects.

Then we consider the statistical distribution of these point defects in the host $BaTiO_3$ crystal. Usually these point defects are thought to be distributed randomly; however, if we are looking at the local (short-range) environment of a given defect, the short-range distribution of other defects around it may show certain statistical symmetry. This is what we call defect symmetry. In a Mn-doped $BaTiO_3$ crystal, the defect symmetry we consider is the symmetry of the short-range distribution of O^{2-} vacancies around a given Mn^{3+} dopant.

Now we show that this defect symmetry conforms to the crystal symmetry when in equilibrium. As $BaTiO_3$ has different crystal symmetry in the paraelectric and ferroelectric states, we will explain this principle separately in the two states.

Above the phase transition point T_C, the crystal is in the paraelectric state and has a cubic symmetry [see Fig. 1(a)]. We now define the conditional probability of finding an O^{2-} vacancy at one of the six O^{2-} sites next to a given Mn^{3+} dopant as the defect probability $P_i^V (i=1–6)$. In the cubic paraelectric structure, the six O^{2-} sites are equivalent for the Mn^{3+} dopant at site 0; thus the defect probability should be the same at the O^{2-} site 1, 2, ..., 6 $(P_1^V=P_2^V=P_3^V=P_4^V=P_5^V=P_6^V)$. This means that defects have cubic symmetry when in equilibrium, which conforms to the cubic crystal symmetry. To simplify the description in the following, we use symbols to represent defect symmetry and crystal symmetry; small square represents the cubic defect symmetry and large squares represents the cubic crystal symmetry, as shown in Fig. 1.

When cooled down below T_C, the crystal changes to the ferroelectric state with a spontaneous polarization $\mathbf{P}_S$ along the $\langle 001 \rangle$ directions due to the relative displacement of positive and negative ions [see Fig. 1(b)]. Crystal symmetry now is tetragonal. However, point defects cannot migrate during this process because the paraelectric-ferroelectric phase transition is diffusionless. Consequently, the defect distribution is the same (cubic symmetry) as in the paraelectric state. That means that for the fresh crystal (immediately after transition), cubic defect symmetry is inherited in the tetragonal crystal symmetry, as shown in Fig. 1(b). The tetragonal crys-
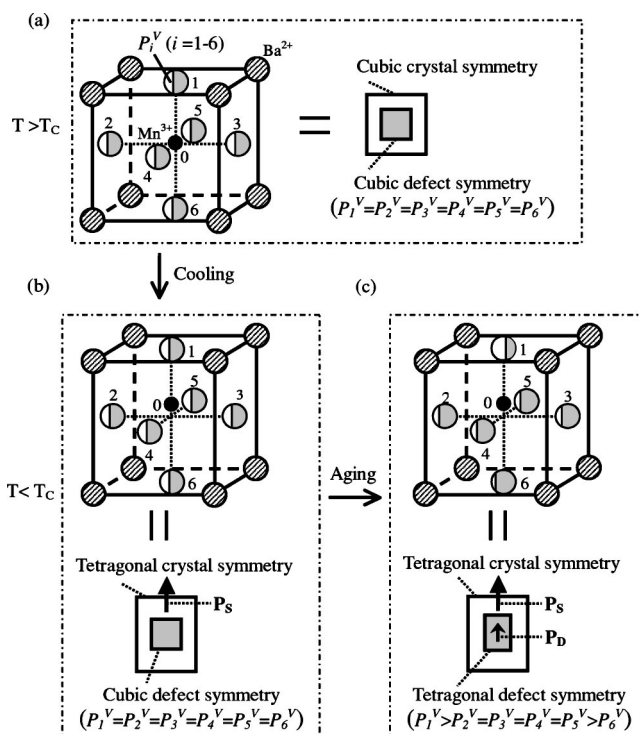

FIG. 1. Defect symmetry and related crystal symmetry in perovskite $BaTiO_3$ structure doped with Mn^{3+} ions at Ti^{4+} sites. (a) Equilibrium paraelectric state, (b) immediately after paraelectric-ferroelectric phase transition at T_C, and (c) equilibrium ferroelectric state (after aging at $T < T_C$). P_i^V refers to the conditional probability of finding an O^{2-} vacancy at O^{2-} site $i(i=1–6)$ next to a given Mn^{3+} ion at site 0. Large square or rectangle represents crystal symmetry, while small square or rectangle represents defect symmetry. Thick arrow refers to spontaneous polarization $\mathbf{P}_S$, and thin arrow refers to defect polarization $\mathbf{P}_D$. T_C is the paraelectric-ferroelectric phase transition temperature.

tal symmetry is represented by the large rectangle, while $\mathbf{P}_S$ is represented by the thick arrow.

However, such a state [Fig. 1(b)] is actually not stable. The reason is that in a tetragonal structure, the six neighboring O^{2-} sites are not equivalent for the Mn^{3+} at site 0: sites 2, 3, 4, and 5 are equivalent, but site 1 is closer and site 6 is farther in distance. It is natural that the closer site should have larger defect probability due to the Coulomb attractive force between the effectively negative Mn^{3+} dopant and the effectively positive O^{2-} vacancy. Therefore, the defect probability should change to $P_1^V > P_2^V=P_3^V=P_4^V=P_5^V > P_6^V$, showing tetragonal symmetry when in equilibrium. However, such a process involves the short-range migration of O^{2-} vacancy (for example, from O^{2-} site 3 to site 1). Consequently, it requires some time to complete; this is the microscopic origin of the aging of the ferroelectric phase (i.e., the phenomenon of the change in properties with time). After the ferroelectric phase has aged for a long time, defect symmetry follows the tetragonal crystal symmetry. The noncentric distribution of charged defects (Mn^{3+} dopant and O^{2-} vacancy) forms defect polarization $\mathbf{P}_D$ along the direction of $\mathbf{P}_S$ [Fig. 1(c)]. The tetragonal defect symmetry is represented by the small rectangle, while $\mathbf{P}_D$ is represented by the thin arrow.

According to the above explanation, we know that aging is the key point to establish such a symmetry-conforming defect configuration. For a crystal aged in the ferroelectric state, defect symmetry follows tetragonal crystal symmetry and $\mathbf{P}_D$ aligns along $\mathbf{P}_S$. Without aging, defect symmetry in the tetragonal crystal symmetry inherits the cubic symmetry of the paraelectric state and $\mathbf{P}_D$ is zero. If an electric field is applied to an aged crystal, its orientation and $\mathbf{P}_S$ can be changed instantaneously, while the defect symmetry and associated $\mathbf{P}_D$ cannot have a sudden change. Therefore, after removing the electric field, the unchanged defect symmetry and the associated $\mathbf{P}_D$ cause a reversible domain switching and consequently produces a macroscopic double-hysteresis loop and a recoverable electrostrain effect. As mentioned in the Introduction, such peculiar macroscopic properties had already been observed in our previous work[4,8] but without the mesoscopic (domain-level) evidence. In the following we present direct mesoscopic evidence behind the macroscopic properties. Furthermore, we compare the different mesoscopic and macroscopic behavior of aged and unaged samples to get some clues about the microscopic (atomic level) information for the observed phenomena.

III. EXPERIMENT

A. Design of experimental setup

In order to verify the domain-switching process behind the macroscopic properties, we designed a special experimental setup as schematically illustrated in Fig. 2.

First, the domain-switching observation and *P-E* hysteresis loop measurement were simultaneously done with the setup shown in Fig. 2(a). The polished sample was painted with air-drying silver electrode on both *lateral* sides. Then it was placed on a transparent glass plate and connected to the voltage output of a ferroelectric tester (Radiant workstation) through a silver conducting channel on the surface of the glass plate. As the contact between the sample and the silver channel is soft, there exists no clamping effect on the sample. The electric field was thus applied along the lateral $\langle 100 \rangle$ direction. The domain switching process was observed with an optical microscope, the object lens of which was set perpendicular to the polished sample surface, which is the $\langle 001 \rangle$ direction. During electric field cycling, the evolution of domain patterns was recorded by a digital camera and transferred to a computer. At the same time the *P-E* hysteresis loop was measured by the ferroelectric tester.

Then the electrostrain of the sample was measured by a photonic sensor during a hysteresis loop measurement,[4] as schematically shown in Fig. 2(b). The sample with electrodes on both surfaces was connected to a ferroelectric tester (Radiant workstation). The electric field was thus applied along the $\langle 001 \rangle$ direction (thickness direction). Above the surface of the sample was the noncontact displacement sensor. During a hysteresis measurement both the hysteresis loop and strain-field curve were obtained.

B. Sample preparation and measurement

The sample used in this experiment was a Mn-doped BaTiO$_3$ single crystal (denoted as Mn-BaTiO$_3$). It was grown
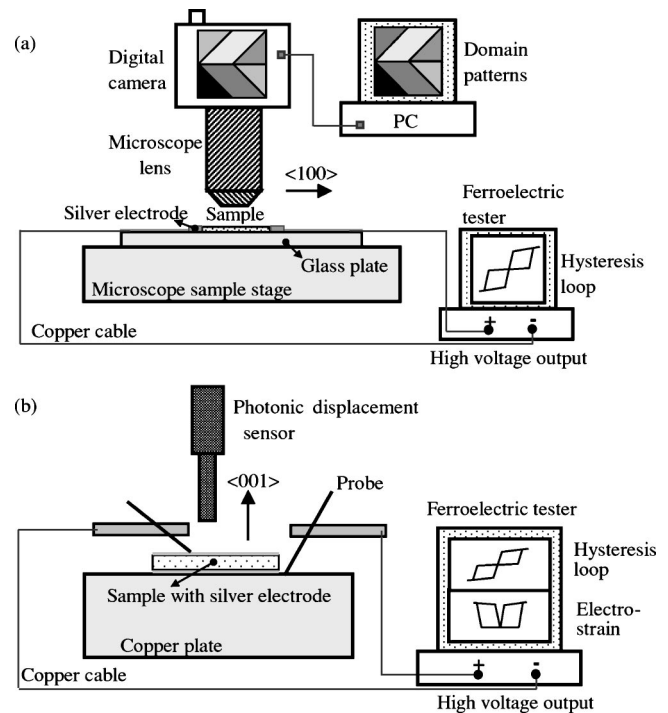

FIG. 2. Experimental setup for (a) simultaneous *in situ* domain observation and hysteresis loop measurement and (b) simultaneous electrostrain and hysteresis loop measurement. In (a), the sample with a lateral electrode was put on a transparent glass plate and connected to the output of a ferroelectric tester by a silver conducting channel. The electric field was thus applied in the transverse direction, while domain observation was performed in the thickness direction. In (b), the sample with a surface electrode was connected to the output of the ferroelectric tester by probes. The electric field was thus applied in the thickness direction and electrostrain was also measured in the thickness direction.

by BaCl$_2$ flux in an Ar atmosphere at about 1300 °C.[12] The valence state of the Mn ion is mostly +3 under such growth conditions.[13] The concentration of Mn ions was determined by electron probe micro-analysis (EPMA) to be about 0.3 mol % relative to the *B*-site Ti ions. The Mn-BaTiO$_3$ crystal was first polished to less than 100 μm thick, heated to above T_C, and kept for 4–5 h. Then it was quickly cooled to room temperature (to avoid aging in the process of cooling from T_C to room temperature). This "fresh" ferroelectric state was taken as the unaged state. On the other hand, *the same sample* was aged at 80 °C (i.e., in the ferroelectric state) for two weeks to establish a fully aged state. We performed *in situ* domain observation on this sample for both the aged and unaged states.

For *in situ* domain observation upon electric field cycling, we applied an electric field of 0.2 Hz, which corresponds to a measurement time of 5 s in one bipolar cycle. In the following, we provide a series of micrographs corresponding to different points of the hystereis loop. As to the subsequent electrostrain measurement, the experiment was performed on the same batch of Mn-BaTiO$_3$ samples as used in the domain observation.
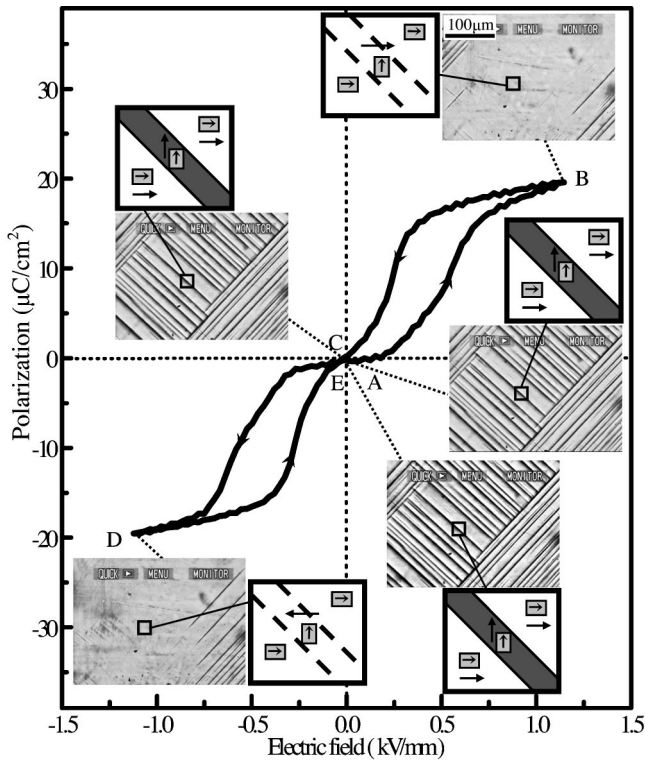
FIG. 3. Direct evidence for reversible domain-switching process and its relation to double hysteresis loop in aged Mn-BaTiO$_3$ single-crystal sample. Beside each micrograph is the schematic configuration of defect symmetry and $\mathbf{P}_S$ state within the part indicated in the micrograph (solid lines inside the schematic graphs A, C, and E show the 90° ferroelectric domain wall, while dotted lines inside the schematic graphs B and D show the "domain wall" of different $\mathbf{P}_D$ configuration formed by defects). See Fig. 1 for the definition of rectangles and arrows. For a video of this process see Ref. 18.

FIG. 4. Irreversible domain-switching process and its relation to normal hysteresis loop in unaged Mn-BaTiO$_3$ single crystal sample. The unaged sample is obtained by deaging the same sample as used in Fig. 3 above T_C and fast cooling to room temperature. Beside each micrograph is the schematic configuration of defect symmetry and $\mathbf{P}_S$ state within the part indicated in the micrograph (solid lines inside the schematic graphs A, C, and E show the ferroelectric domain walls). See Fig. 1 for the definition of square and arrow. See a video of this process at.[19]

IV. RESULTS

A. *In situ* microscopy observation of domain patterns during electric field cycling: Contrasting behavior of aged and unaged samples

In the following, we show in Figs. 3 and 4 the micrographs of domain patterns during electric field cycling and the corresponding P-E hysteresis loop for aged and unaged Mn-BaTiO$_3$ single crystals, respectively. Beside each micrograph, the corresponding defect symmetry state and $\mathbf{P}_S$ state is also illustrated; but this will be discussed later. Here we only show the experimental observation.

First, we examined the domain-switching behavior of aged samples. For the aged multidomain sample, the average polarization equals zero, corresponding to point A in the hysteresis loop curve (see Fig. 3). When an electric field is applied, domain switching occurs, leading to a gradual increase of polarization. When the field reaches maximum, an almost single-domain configuration is observed, which corresponds to the maximum polarization (point B in the P-E curve). Interestingly, when the electric field decreases to zero, we observed the same multidomain pattern as the original one (compare the micrograph at points A and C). At the same time, the averaged macroscopic polarization becomes zero
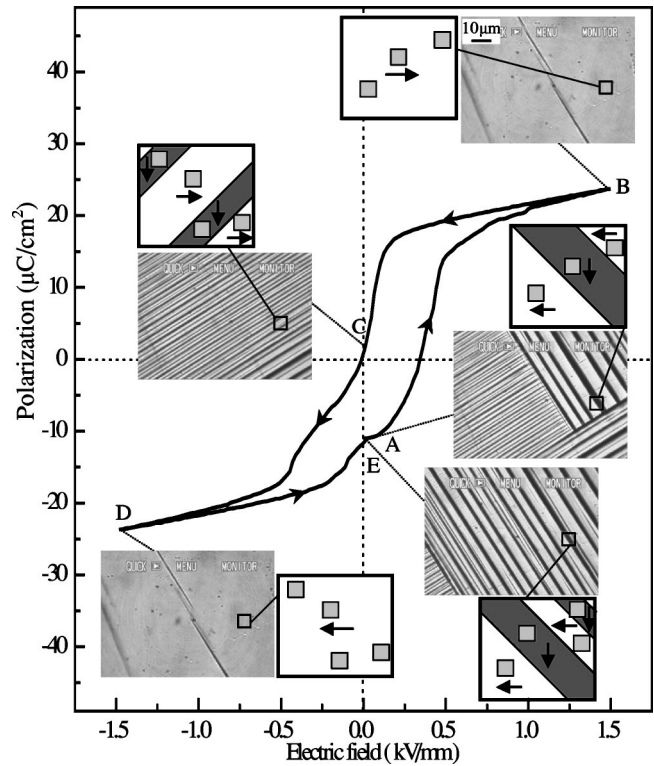
(point C in the P-E curve). Furthermore, the same is true for the reverse electric field except that the polarization changes to negative (see C-D-E cycle in Fig. 3). The whole process can be found in our video.[18] Thus, we observed an interesting reversible domain-switching process during electric field cycling in the aged sample. It corresponds well to the peculiar double P-E hysteresis loop.

By comparison, when an electric field is applied to the unaged sample, a different domain-switching behavior is observed as shown in Fig. 4. (Here the unaged sample is the same sample as the above one, but after a "deaging" by heating to above T_C, keeping 4–5 h, then fast cooling to room temperature.) We start from the point A that has a negative averaged polarization in the P-E curve. With increasing electric field, domain switching contributes to the increase of polarization. At maximum electric field, a single-domain state is observed, and simultaneously polarization increases to maximum (point B in the P-E curve). However, when the electric field decreases to zero, another domain pattern, which is totally different from the original one, is observed (compare the micrograph at points A and C). At the same time, polarization does not come back to zero and stays at a positive value (point C). Moreover, in reverse field cycling, another different domain configuration is observed and
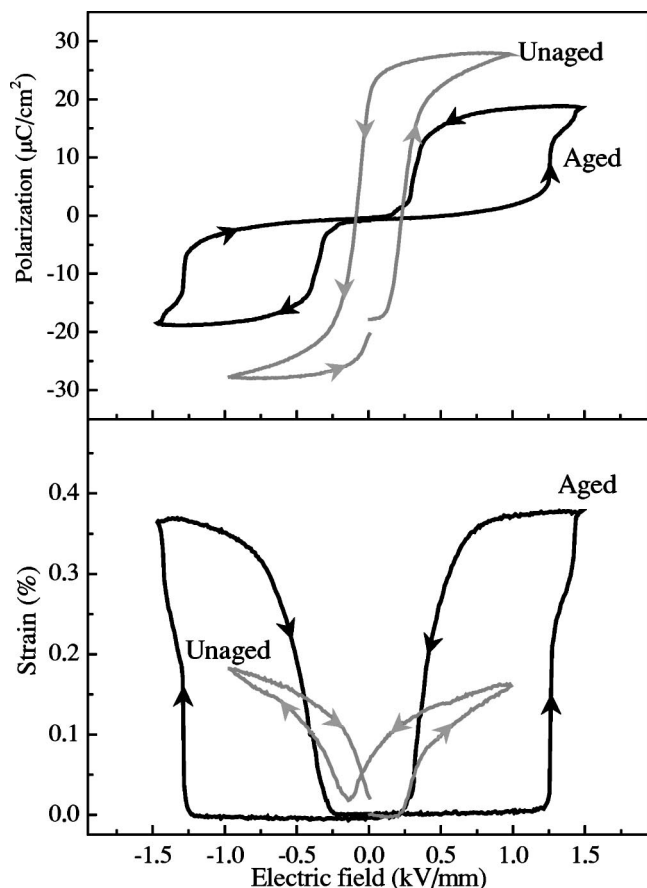
FIG. 5. Contrasting *P-E* hysteresis loop and electrostrain behavior between aged Mn-BaTiO$_3$ (solid line) and unaged Mn-BaTiO$_3$ (dotted line). The aged sample shows a double hysteresis loop and recoverable electrostrain; the unaged sample shows normal hysteresis loop and butterfly-type electrostrain.

the polarization keeps the negative nonzero value (see the *C-D-E* cycle in Fig. 4). The whole process can be found in our video.[19] We consequently observed that domain switching in the unaged sample is an irreversible process during electric field cycling. It corresponds to the well-known normal hysteresis loop.

B. Electrostrain behavior associated with domain-switching process in aged and unaged samples

Now we show another important macroscopic consequence accompanying the domain-switching process, the electrostrain behavior. This experimental result is shown in Fig. 5.

The black line in Fig. 5 shows the strain vs electric field curve and the corresponding *P-E* hysteresis loop for the aged sample. The curves show that with the electric field increasing to maximum, polarization increases to maximum due to domain switching (recall Fig. 3); and simultaneously strain also increases to the maximum value. When the field is removed, the averaged polarization becomes zero, which is consistent with the restoration of the original multidomain state as shown in Fig. 3. At the same time, the strain also recovers to zero. The same is true for the reverse electric

field. Thus we observed an interesting recoverable electrostrain corresponding to a double hysteresis loop, which also corresponds to the reversible domain-switching process in Fig. 3. We noticed there is some difference in the coercive field E_C between the sample used in the electrostrain measurement and that in the domain observation. This is attributed to the different Mn concentration of different samples although they are from the same batch of single crystals grown in the same crucible.

However, the unaged sample (obtained after deaging the aged sample at above T_C and then fast cooling down to room temperature), in contrast to the aged one, shows a different strain vs field curve (gray line in Fig. 5). When an electric field is applied, strain increases with increasing polarization. However, when the field decreases to zero, the polarization has a remanence due to the irreversible domain switching (recall Fig. 4); the strain level also does not recover to zero, and there exists some remanant strain. The strain recovers to zero only on applying a suitable reverse electric field. This gives the well-known irrecoverable butterfly-type electrostrain behavior during field cycling. It corresponds to the normal hysteresis loop and to irreversible domain switching as shown in Fig. 4.

Up to now, our experiments have correlated the mesoscopic domain-switching process with macroscopic properties like the hysteresis loop and electrostrain. Through the experimental results on the aged sample, we confirmed that the reversibility of the domain-switching process is responsible for the macroscopic recoverable electrostrain behavior. This gives direct mesoscopic evidence for our reversible domain-switching mechanism. On the other hand, through comparison with the different behavior of the unaged sample, we confirmed that reversible domain switching stems from aging in the ferroelectric state. As aging causes a symmetry-conforming configuration of the defects (discussed in Fig. 1), all these observations suggest the central role of microscopic defect symmetry in determining mesoscopic domain-switching behavior and macroscopic polarization and strain behavior. This will be discussed in detail in the following section.

V. DISCUSSION

A. Relation among microscopic defect symmetry, mesoscopic domain-switching behavior, and macroscopic ferroelectric and electrostrain properties

Now we explain the microscopic origin of the mesoscopic domain-switching behavior and associated macroscopic properties in aged and unaged samples from the viewpoint of defect symmetry.

As we know, a ferroelectric crystal cooled from a high temperature (paraelectric state) naturally shows multidomain patterns. For a multidomain sample, after aging in the ferroelectric state, as discussed in Sec. II, the defect symmetry follows the tetragonal crystal symmetry and the defect polarization $\mathbf{P}_D$ aligns along the direction of $\mathbf{P}_S$ within each domain according to the defect symmetry principle[4,8] (see Fig. 3). When the electric field is applied, $\mathbf{P}_S$ is switched to the direction of the electric field and domain switching occurs.

This leads to an increase of polarization and strain. At maximum electric field, a single-domain state is obtained. Simultaneously, polarization and strain reach maximum values. However, defect symmetry and the associated $\mathbf{P}_D$ cannot be rotated during such a diffusionless domain-switching process. This unswitched defect symmetry and associated $\mathbf{P}_D$ consequently provide a restoring force favoring a reversible domain switching. Thus after removing the external field, the switched domain restores the original domain orientation by defect symmetry and $\mathbf{P}_D$. Therefore, the most important consequence of the defect symmetry principle is that the defect symmetry and $\mathbf{P}_D$ can memorize the original crystal domain patterns after aging, and do not change during subsequent domain switching. This assures that $\mathbf{P}_S$ can be switched back to the original orientation so that defect orientation follows crystal orientation and $\mathbf{P}_D$ aligns along $\mathbf{P}_S$ in every domain. As a result, the averaged polarization and strain become zero (black line in Fig. 5). This results in reversible domain switching during electric field cycling (Fig. 3) and a corresponding double *P-E* hysteresis loop as well as a recoverable electrostrain (black line in Fig. 5) in the aged sample.

On the other hand, without aging (i.e., immediately after the paraelectric-ferroelectric transition), point defects in the tetragonal ferroelectric phase inherit the same defect symmetry (cubic) as the cubic paraelectric phase because the transition is diffusionless and involves no exchange of ions. Therefore, for an unaged multidomain sample, the defect symmetry is cubic with zero defect polarization in every domain (see Fig. 4). When an electric field is applied, $\mathbf{P}_S$ is switched to the direction of the field, and thus a single-domain state is obtained at maximum electric field. At the same time, the polarization and strain increase to maximum. During such a process, the defect symmetry remains cubic. This cubic defect symmetry with a zero defect polarization does not favor any particular domain state. Consequently, when the field decreases to zero, the single-domain state should remain unchanged, as there is no force to reverse the switched domain to the original state. Nevertheless, because of the inevitable existence of the depolarization field, the single-domain state will change into a multidomain state, but this multidomain state has no relation to the initial multidomain state, as observed in Fig. 4. Correspondingly, the polarization and strain do not recover to zero (gray line in Fig. 5). Thus the domain-switching behavior in the unaged sample is irreversible during electric field cycling (Fig. 4). This corresponds to the normal hysteresis loop and butterfly-type electrostrain (gray line in Fig. 5).

Now based on the defect symmetry principle, the domain switching and corresponding macroscopic properties of both aged and unaged samples can be well understood. The contrasting behaviors of aged and unaged samples further support our proposal that reversible domain-switching behavior is closely related to the change of defect symmetry during aging. Such a microscopic mechanism is responsible for the observed mesoscopic reversible domain-switching process, the macroscopic double hystersis loop, and the recoverable electrostrain effect.
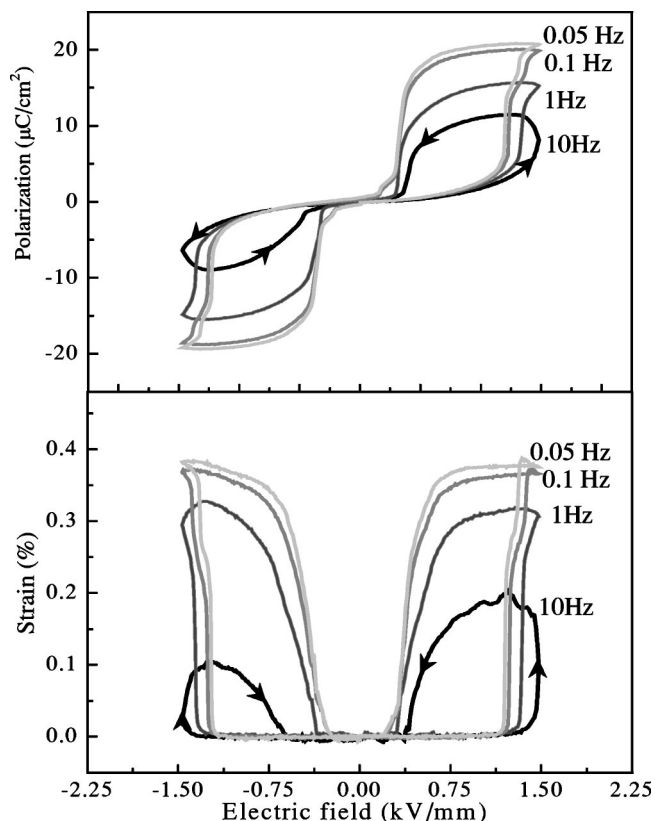

FIG. 6. Dependence of *P-E* hysteresis loop and electrostrain on field frequency in the aged Mn-BaTiO$_3$ sample. The electrostrain shows strong recoverability over a wide frequency range.

B. Frequency dependence of the recoverable electrostrain effect

As discussed above, the restoring force of reversible domain switching is provided by the symmetry-conforming property of defects. On the other hand, the symmetry-conforming configuration of defects can be changed by the migration of O^{2-} vacancies in neighboring O^{2-} sites. Such migration is quite possible when we apply a large electric field (large force on effectively charged vacancies), or when we do field cycling at sufficiently low frequency (longer time for migration). Consequently the restoring force will be changed due to the migration of O^{2-} vacancies. This change will affect the reversibility of domain switching and consequently the recoverable electrostrain. Therefore, it is necessary to further investigate the dependence of the recoverable electrostrain effect on field frequency. This is discussed in the following.

The *P-E* hysteresis loop and electrostrain in aged Mn-BaTiO$_3$ single-crystal samples at a field frequency ranging from 10 to 0.05 Hz are shown in Fig. 6. From this figure, it is found that the double hysteresis loop and recoverable electrostrain persist even down to the low frequency of 0.05 Hz. This result indicates that the restoring force from point defects, which is responsible for the double hysteresis loop and recoverable electrostrain, is very strong. Thus we can expect a wide frequency range of this recoverable electrostrain ef-

fect. This is important for the application of this effect.

Moreover, we notice that with decreasing frequency polarization increases from 10 to 20 $\mu C/cm^2$ and electrostrain increases from 0.15% to 0.4%. These interesting phenomena can be explained as follows. When the frequency of electric field cycling is lower (that is, the measurement time becomes longer), some O^{2-} vacancies migrate along the direction of the electric field (e.g., jump from site 3 to site 1 in Fig. 1). Therefore, the number of defects staying in the original state becomes fewer. This makes domain switching easier because there is less resistance from point defects. Therefore, at the same electric field but with lower frequency, more domains can be switched, thus leading to a larger polarization and electrostrain. However, the recoverability becomes weaker. This is because fewer defects stay in the original state; they provide a weak restoring force for reverse domain switching. When the frequency is lower than 0.1 Hz, the strain value becomes saturated, indicating a maximum of switched domains. Therefore, the field frequency dependence of recoverable electrostrain also can be well understood by our defect-mediated reversible domain-switching mechanism.

C. Comparison of our mechanism with others

Our defect-mediated reversible domain-switching mechanism explains the observed aging-induced double *P-E* hysteresis loop and the corresponding recoverable electrostrain effect in a consistent way, and is supported by all existing experimental evidence. On the other hand, historically, the strange aging-related double *P-E* hysteresis loop was also reported in various ferroelectric systems[13–15] (but without realizing the recoverable electrostrain effect). A number of mechanisms have been proposed to explain this phenomenon but without consensus. In the following, we give a critical comparison between our mechanisms and others. As our mechanism has been discussed in detail in the above, now we discuss the previous ones and compare them with ours.

First we briefly introduce the previously proposed models, including the grain boundary effect,[15] the domain-wall pinning effect,[16] and the volume effect.[13,17] Generally, all these models agree that defects play a decisive role in the aging-related phenomena. However, they differ much in the driving force for defect migration. In the grain boundary model, defects form a second phase and locate at the grain boundary. They collect surface charges to compensate for the polarization discontinuities and lower depolarization energy. Thus, the existing domain configuration is stabilized by the collected charges. In the domain-wall pinning model, defects migrate to the highly stressed domain walls to lower the domain-wall energy; thus the domain wall is pinned by the defects. As to the volume model,[13,17] it is considered that polar lattice defects are reoriented with respect to the direction of spontaneous polarization in bulk materials during aging. Therefore, the polarization is stabilized by defect dipoles. Therefore, all these models seem to be able to provide a self-consistent explanation of the double hysteresis loop in aged ferroelectric crystals.

However, the grain boundary model and domain-wall pinning model encounter the following difficulties with respect to our experimental results. First, our experiment showed that perfect double *P-E* hysteresis loop exists in the aged *single-crystal* sample. This cannot be explained by grain boundary effect, as the single crystal has no grain boundary. Second, we observed that domain walls are displaced by a macroscopic distance (at least an order of a millimeter; see Fig. 3) and an almost single-domain state is formed; yet, *the original multidomain pattern can still be restored from this single-domain state* after removing the electric field. The extremely long-range reversibility is difficult explain by the domain-wall pinning effect, as the pinning force is known to be of very short-range nature and thus it is hard to drag back a macroscopically displaced domain wall. Moreover, the domain-wall pinning effect cannot explain the restoration of the initial multidomain state from a single-domain state because there would be no domain wall to be dragged back. Our experimental results can only be explained by a volume effect, as only the stabilization of $\mathbf{P}_S$ by defects distributed in the whole volume can provide a strong restoring force and assure the restoration of original domain patterns even from a single-domain state. In this respect, the volume effect proposed by Lambeck *et al.*[13,17] seems most relevant, as it can overcome the difficulty with the boundary effect model. However, this model is based on a key assumption that there exist dipolar defects and they follow $\mathbf{P}_S$ after aging. This assumption is not verified within their model. However, our mechanism, which also is a volume effect, provides a microscopic explanation for the origin of aging, and it involves no assumption. The conformation of the defect dipole with spontaneous polarization naturally comes from the symmetry-conforming property of the defects, as shown in Fig. 1. In addition, the symmetry of the statistical distribution of defects also provides a restoring force for the reversible domain switching, which is not considered in the model of Lambeck *et al.*

Based on the above discussions, we believe that reversible domain switching in aged sample stems from the defect symmetry principle. This model is advantageous over other models in that it provides a *microscopic mechanism* (without *a priori* assumptions) for all the observed phenomena at different scales, including the mesoscopic domain-switching behavior and the macroscopic *P-E* hysteresis loop and electrostrain effect.

VI. CONCLUSIONS

We performed an *in situ* study on domain pattern evolution during electric field cycling for Mn-doped $BaTiO_3$ single crystals. The following conclusions are obtained.

(1) For aged samples, a reversible domain-switching process was observed, which corresponds well to the macroscopic double *P-E* hysteresis loop and recoverable electrostrain effect. This provides a direct mesoscopic evidence for the reversible domain-switching mechanism of the giant recoverable electrostrain effect.

(2) The same sample in an unaged state showed an irreversible domain switching corresponding to the normal *P-E* hysteresis loop and unrecoverable butterfly-type electrostrain effect. This indicates that reversible switching in

aged samples is closely related to defect migration during aging.

(3) The contrasting behavior of aged and unaged samples suggests that the microscopic mechanism of all the mesoscopic domain behavior and macroscopic hysteresis and electrostrain behavior stems from the symmetry-conforming property of point defects.

(4) We further found that recoverable electrostrain is available even down to very low frequency due to the strong restoring force from point defects. This is important for the application of the giant recoverable electrostrain effect.

(5) Our results suggested that aging is a volume effect, rather than a boundary pinning effect.

ACKNOWLEDGMENTS

---

*Corresponding author. Electronic address: ren.xiaobing@nims.go.jp

[1] F. Jona and G. Shirane, *Ferroelectric Crystals* (Macmillan, New York, 1962).

[2] K. Uchino, *Ferroelectric Device* (Marcel Dekker, New York, 2000).

[3] S. E. Park and T. R. Shrout, J. Appl. Phys. **82**, 1804 (1997).

[4] X. Ren, Nat. Mater. **3**, 91 (2004).

[5] X. Ren and K. Otsuka, Nature (London) **389**, 579 (1997).

[6] X. Ren and K. Otsuka, Phys. Rev. Lett. **85**, 1016 (2000).

[7] X. Ren and K. Otsuka, MRS Bull. **27**, 15 (2002).

[8] L. X. Zhang, W. Chen, and X. Ren, Appl. Phys. Lett. **85**, 5658 (2004).

[9] J. A. Hooton and W. J. Merz, Phys. Rev. **98**, 409 (1955).

[10] P. W. Forsbergh, Phys. Rev. **76**, 1187 (1949).

[11] D. M. Smyth, *The Defect Chemistry of Metal Oxides* (Oxford University Press, New York, 2000).

[12] A. Feltz and H. Langbein, Krist. Tech. **6**, 359 (1971).

[13] P. V. Lambeck and G. H. Jonker, J. Phys. Chem. Solids **47**, 453 (1986).

[14] W. A. Schulze and K. Ogino, Ferroelectrics **87**, 361 (1988).

[15] K. Carl and K. H. Hardtl, Ferroelectrics **17**, 473 (1978).

[16] V. S. Postnikov, V. S. Pavlov, and S. K. Turkov, J. Phys. Chem. Solids **31**, 1785 (1970).

[17] U. Robels and G. Arlt, J. Appl. Phys. **73**, 3454 (1993).

[18] http://www.nims.go.jp/ferroic/domain/reversible/htm

[19] http://www.nims.go.jp/ferroic/domain/irreversible/htm